Kinetic and Thermodynamic Analysis of the Interaction of Cations with Dialkylglycine Decarboxylase†

Wenshe Liu and Michael D. Toney*

Department of Chemistry, University of California − Davis, Davis, California 95616

Received October 14, 2003; Revised Manuscript Received December 30, 2003

ABSTRACT: Dialkylglycine decarboxylase (DGD) is a tetrameric pyridoxal phosphate (PLP)-dependent enzyme that catalyzes both decarboxylation and transamination in its normal catalytic cycle. Its activity is dependent on cations. Metal-free DGD and DGD complexes with seven monovalent cations (Li^+, Na^+, K^+, Rb^+, Cs^+, NH_4^+, and Tl^+) and three divalent cations (Mg^{2+}, Ca^{2+}, and Ba^{2+}) have been studied. The catalytic rate constants for cation-bound enzyme (ck_{cat} and ck_{cat}/bK_{AIB}) are cation-size-dependent, K^+ being the monovalent cation with the optimal size for catalytic activity. The divalent alkaline earth cations (Mg^{2+}, Ca^{2+}, and Ba^{2+}) all give ∼10-fold lower activity compared to monovalent alkali cations of similar ionic radius. The Michaelis constant for aminoisobutyrate (AIB) binding to DGD−PLP complexes with cations (bK_{AIB}) varies with ionic radius. The larger cations (K^+, Rb^+, Cs^+, NH_4^+, and Tl^+) give smaller bK_{AIB} (∼4 mM), while smaller cations (Li^+, Na^+) give larger values (∼10 mM). Cation size and charge dependence is also found with the dissociation constant for PLP binding to DGD−cation complexes (aK_{PLP}). K^+ and Rb^+ possess the optimal ionic radius, giving the lowest values of aK_{PLP}. The divalent alkaline earth cations give aK_{PLP} values ∼10-fold higher than alkali cations of similar ionic radius. The cation dissociation constant for DGD−PLP−AIB−cation complexes ($\beta K_{M^{z+}}$) was determined and also shown to be cation-size-dependent, K^+ and Rb^+ yielding the lowest values. The kinetics of PLP association and dissociation from metal-free DGD and its complexes with cations (Na^+, K^+, and Ba^{2+}) were analyzed. All three cations tested increase PLP association and decrease PLP dissociation rate constants. Kinetic studies of cation binding show saturation kinetics for the association reaction. The half-life for association with saturating Rb^+ is ∼24 s, while the half-life for dissociation of Rb^+ from the DGD−PLP−AIB−Rb^+ complex is ∼12 min.

Monovalent cations such as K^+, Na^+, or NH_4^+ participate in a variety of biological processes. However, in contrast to the rather specific functions that may be assigned to certain divalent cations such as Mg^{2+} and Ca^{2+}, the mode of action of monovalent cations is poorly defined. Early reviews by Evan and Sorger and Suelter gave compilations of enzymes requiring monovalent cations for activation (*1*−*3*). They were able to generalize that enzymes activated by K^+ are also usually activated by Rb^+ and NH_4^+ but only poorly by Na^+ and not at all by Li^+. A few enzymes activated by Na^+ are also activated by Li^+ but are activated much less or not at all by K^+, Rb^+, and NH_4^+. A more recent review by Woehl and Dunn focused on pyridoxal phosphate (PLP)[1]-dependent enzymes and proposed two types of mechanisms to explain the effects of metal ions on the catalytic activity (*4*). The first invokes the metal ion in a static structural role wherein binding activates the enzyme by simply stabilizing the catalytically active conformation of the protein. The second proposes that the metal ion plays a dynamic role with binding selectively assisting one or more of the protein conformational transitions essential to catalysis. One of the three PLP-dependent enzymes examined in this latter review is 2,2-dialkylglycine decarboxylase (DGD).

DGD is found in the bacterium *Pseudomonas cepacia*, in the wheat blotch fungus *Mycospheaerella graminicola*, and in other fungi and bacteria (*5*, *6*). It is an unusual PLP-dependent enzyme that combines both decarboxylation and transamination half-reactions in its normal catalytic cycle (Scheme 1) and that has been characterized kinetically and structurally (*7*−*11*). It is tetrameric, best described as a dimer of dimers. The active sites are shared between subunits in the dimeric structure.

Previous work has shown that large monovalent cations such as K^+, Rb^+, and NH_4^+ activate DGD while small monovalent cations, Li^+ and Na^+, are inhibitory (*5*). Toney et al. identified two metal ion binding sites in each DGD monomer based on X-ray crystallographic analyses (*7*, *12*). Site 2 is on the surface and is specific for binding Na^+.

† Supported by Grant GM54779 to M.D.T. from the National Institutes of Health. W.L. was supported by Grant 2001-07 of the University of California Systemwide Biotechnology Research Program.

* To whom correspondence should be addressed. E-mail: mdtoney@ucdavis.edu. Tel: 530-754-5282. Fax: 530-752-8995.

[1] Abbreviations used: PLP, pyridoxal-5′-phosphate; DGD, 2,2-dialkylglycine decarboxylase; DGD−PLP, PLP form of DGD; DGD−Li, Li^+ complex of DGD−PLP; DGD−Na, Na^+ complex of DGD−PLP; DGD−K, K^+ complex of DGD−PLP; DGD−Rb, Rb^+ complex of DGD−PLP; DGD−Cs, Cs^+ complex of DGD−PLP; DGD−NH_4, NH_4^+ complex of DGD−PLP; DGD−Tl, Tl^+ complex of DGD−PLP; DGD−Mg, Mg^{2+} complex of DGD−PLP; DGD−Ca, Ca^{2+} complex of DGD−PLP; DGD−Ba, Ba^{2+} complex of DGD−PLP; apoDGD, DGD without PLP bound; 2°ADH, NADPH-dependent secondary alcohol dehydrogenase; TEA, triethanolamine; AIB, aminoisobutyrate; DCIP, 2,6-dichlorophenolindophenol.

10.1021/bi035854l CCC: $27.50
Published on Web 04/09/2004

Scheme 1: Half-Reactions Catalyzed by Dialkylglycine Decarboxylase

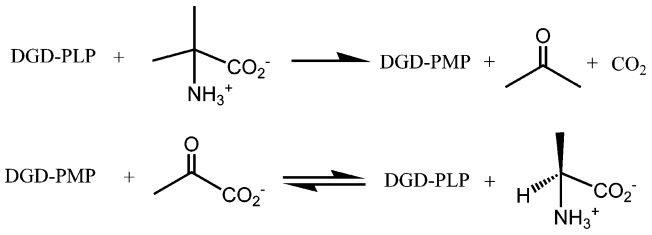

However, site 1 is close to the active site and can bind a variety of cations (Figure 1). A comparison of DGD complexes with K^+ and Na^+ shows that the protein structure in the vicinity of site 1 undergoes a conformational change when Na^+ is substituted for K^+. The conformational change causes a ~1° rotation of the subunits with respect to each other and is believed to be directly linked to the effects of these two metal ions on the activity of the enzyme. Hohenester et al. (*13*) additionally determined the structures of the DGD complexes with Li^+ and Rb^+. They found that Li^+ produces the conformation favored by Na^+ and Rb^+ produces the conformation favored by K^+. Therefore the switch between these two forms is a cation-size-dependent phenomenon.

This study presents a detailed investigation of cation effects on the kinetic parameters for the DGD-catalyzed decarboxylation-dependent transamination reaction between AIB and pyruvate. It is found that all of the binding and rate constants are cation-size- and charge-dependent, K^+ being the favored ion in all cases. The degree of discrimination among the different ions is small compared to other systems, such as valinomycin and K^+ channels, to which DGD is compared in the following. The origin of the differences in discrimination in these systems is considered.

EXPERIMENTAL PROCEDURES

Materials. Succinic acid, TEA, NaOH, KOH, NH_4OH, $MgCl_2$, $CaCl_2$, and $BaCl_2$ were purchased from Fisher. LiOH, RbOH, CsOH, TlCl, and DCIP were obtained from Aldrich. PLP, AIB, pyruvic acid, NADPH, NAD^+, 2°ADH, alanine dehydrogenase, and diaphorase were from Sigma. Dilithium succinate, disodium succinate, dipotassium succinate, dirubidium succinate, dicesium succinate, and diammonium succinate were made by titrating LiOH, NaOH, KOH, RbOH, CsOH, and NH_4OH with succinic acid to pH 7.8.

Apoenzyme Preparation. DGD was expressed and purified according to a literature procedure (*14*). ApoDGD was prepared by reacting DGD with an excess of AIB for 2 h and then dialyzing overnight against 100 mM TEA−succinate, pH 7.8. Apoenzyme concentration was determined with the Bio-Rad DC assay, using IgG as standard and subtracting the TEA background.

Steady-State Kinetic Assay. Two different coupling systems were used in steady-state kinetic assays of DGD. When PLP concentrations were lower than 500 μM, AIB decarboxylation was followed by coupling acetone produced from AIB to the 2°ADH reaction as described previously (*9*). The decrease in NADPH absorbance at 340 nm that occurs during reduction of acetone to 2-propanol was monitored. However, PLP also absorbs at 340 nm, limiting the utility of this assay to relatively low concentrations of PLP. When PLP concentrations were higher than 500 μM, L-alanine produced from pyruvate in the transamination half-reaction was coupled to alanine dehydrogenase. The NADH generated from alanine/NAD^+ in this reaction was coupled to the reduction of DCIP catalyzed by diaphorase. The decrease in DCIP absorbance at 600 nm was monitored. Because pyruvate is an inhibitor of alanine dehydrogenase, this assay was performed at low pyruvate concentrations.

Determination of k_{cat}, K_{AIB}, and K_{PLP} of Metal-Free Enzyme. ApoDGD was prepared as above. ApoDGD (0.3 μM) was incubated with six different concentrations of PLP in 1 mL solutions containing 100 mM TEA−succinate, pH 7.8, 200 μM NADPH, and 1 unit/mL 2°ADH for 2 h. The reactions were initiated by addition of TEA−pyruvate and AIB in a small volume to a final concentration of 2 mM for pyruvate and varying AIB. The initial reaction rates were recorded within ~1 min of initiation.

Determination of bK_{AIB} and ck_{cat} of DGD−Li, DGD−Na, DGD−K, DGD−Rb, DGD−Cs, DGD−NH_4, DGD−Tl, and DGD−Ba. For DGD−K, 0.06 μM apoDGD was incubated with 500 μM PLP and 100 mM dipotassium succinate in 1 mL solutions containing 100 mM TEA−succinate, pH 7.8, 200 μM NADPH, and 1 unit/mL 2°ADH for 1.5 h. The reactions were initiated by addition of TEA−pyruvate and AIB in a small volume to a final concentration of 2 mM pyruvate and varying AIB. The initial rates were recorded. Similar experiments were carried out for DGD−Li, DGD−Na, DGD−Rb, DGD−Cs, DGD−NH_4, DGD−Tl, and DGD−Ba. In these experiments, 100 mM succinate salt of each of these cations, except Tl^+ and Ba^{2+}, was incubated with apoDGD and varying concentrations of DGD were used to obtain reliable data. Since the succinate salts of Tl^+ and Ba^{2+} were not available, 15 mM TlCl was used to incubate apoDGD because of its low solubility, and 100 mM $BaCl_2$ was used because of precipitation with PLP at higher concentrations.

Determination of ck_{cat} and bK_{AIB} of DGD−Mg and DGD−Ca. ApoDGD (4.0 μM) was incubated for 2 h with 3.5 mM PLP and 200 mM $MgCl_2$ or $CaCl_2$ in 1 mL reactions of the following composition: 100 mM TEA−succinate, pH 7.8, 5 units/mL alanine dehydrogenase, 0.2 mM TEA−pyruvate, 20 units/mL diaphorase, and 250 μM DCIP. The reactions were initiated by addition of AIB to varying final concentrations. The decrease of DCIP absorbance at 600 nm was monitored.

Determination of aK_{PLP} for All Cations. For DGD−K, apoDGD was incubated with varying concentrations of PLP and 100 mM dipotassium succinate in 1 mL solutions containing 100 mM TEA−succinate, pH 7.8, 200 μM NADPH, and 1 unit/mL 2°ADH for 1.5 h. The reactions were initiated by addition of substrates in a small volume to a final concentration of 2 mM pyruvate and 0.2 mM AIB. Because AIB concentration was only 1/10 of bK_{AIB} for DGD−K, it did not significantly change the equilibrium between apoDGD−K, PLP, and DGD−K. Similar experiments were carried out for DGD−Li, DGD−Na, DGD−Rb, DGD−Cs, DGD−NH_4, DGD−Tl, DGD−Ca, and DGD−Ba. The concentration of the cation used in incubations with apoDGD was 200 mM for Li^+, Na^+, Rb^+, Cs^+, NH_4^+, and Ca^{2+}, 15 mM for Tl^+, and 100 mM for Ba^{2+}. The AIB concentration used was 1/10 of bK_{AIB} for the DGD complex with the designated cation. For DGD−Mg, apoDGD was

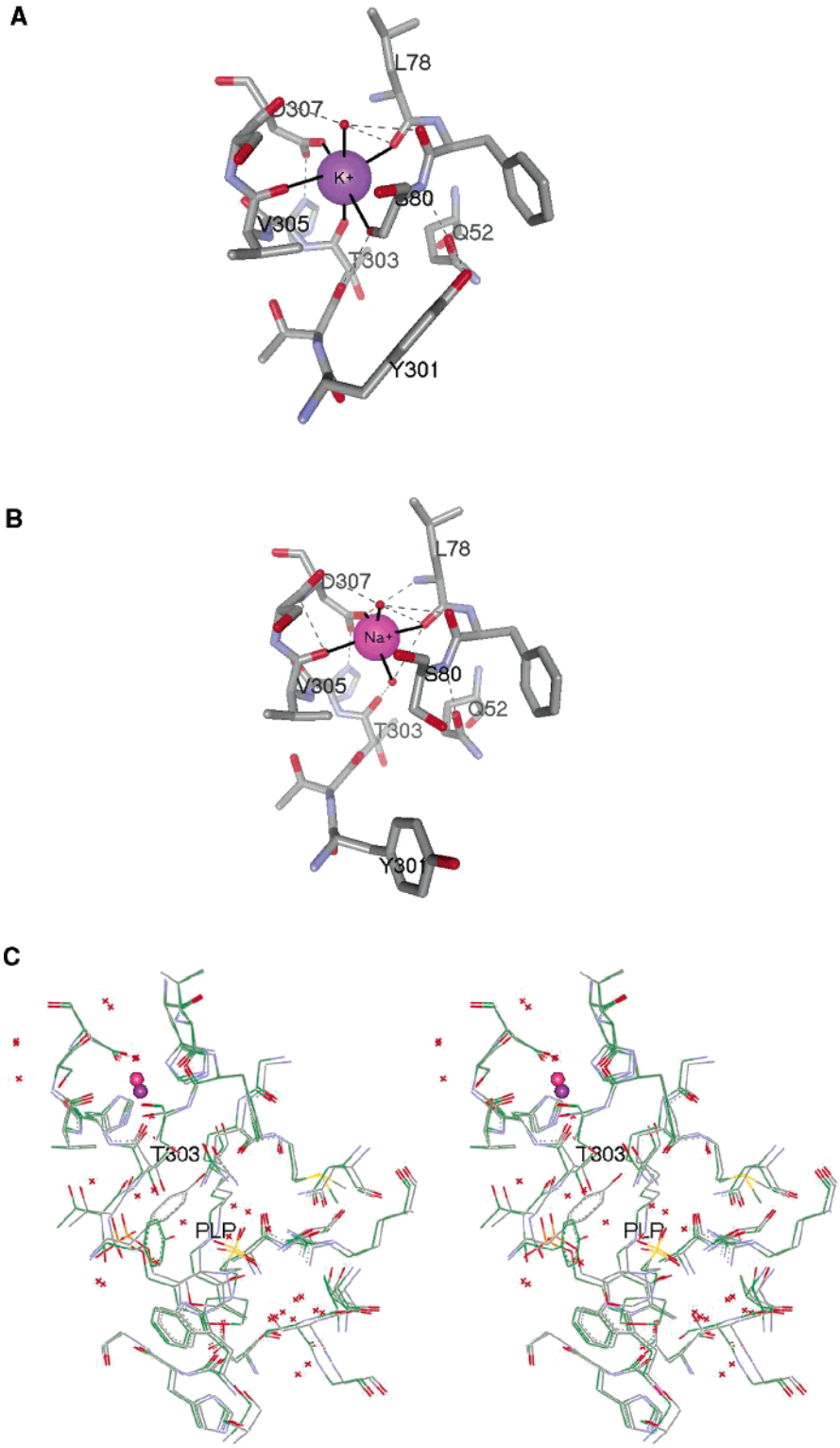

FIGURE 1: Structure of the DGD metal ion binding site 1 (A) with K^+ bound and (B) with Na^+ bound and (C) overlay of the active site and metal ion binding site 1 regions of DGD−K and DGD−Na.

incubated with varying concentrations of PLP and 200 mM $MgCl_2$ in 100 mM TEA−succinate, pH 7.8, 0.2 mM TEA−pyruvate, 5 units/mL alanine dehydrogenase, 5 mM NAD^+, 20 units/mL diaphorase, and 250 μM DCIP for 1.5 h. The reactions were initiated by addition of AIB to a final concentration of 0.6 mM. The decrease of DCIP absorbance at 600 nm was monitored.

Determination of $\beta K_{M^{z+}}$ for All Cations. For DGD−K, apoDGD was incubated with 3.5 mM PLP and varying concentrations of dipotassium succinate in 100 mM TEA−succinate, pH 7.8, for 1.5 h. The reactions were initiated by addition of a small volume of this incubated DGD into 1 mL solutions of the following composition: 100 mM TEA−succinate, same concentrations of dipotassium succinate as that in incubating solutions, 50 mM AIB, 0.2 mM TEA−pyruvate, 5 units/mL alanine dehydrogenase, 5 mM NAD^+, 20 units/mL diaphorase, and 250 μM DCIP. The decrease of DCIP absorbance at 600 nm was monitored over 20 min.

Reaction rates were obtained from the slope of the linear portion for the curves ~15 min after initiation. Similar experiments were carried out for DGD−Li, DGD−Rb, DGD−NH_4, DGD−Tl, DGD−Mg, DGD−Ca, and DGD−Ba. For DGD−NH_4, 25 units/mL alanine dehydrogenase was used since NH_4^+ inhibits it. The activities of DGD−Na and DGD−Cs are close to that of metal-free DGD. To enhance the activity difference between DGD before and after addition of Na^+ or Cs^+, 0.5 mM dipotassium succinate was added into the incubation solutions and reaction solutions. Because K^+ is an activator of DGD and K^+ was at subsaturating concentration, DGD was partially activated. The added Na^+ or Cs^+ competes with K^+ to bind DGD and lower the observed activity. The reaction rates were recorded 15 min after initiation for the reactions.

Rate of PLP Binding to Metal-Free ApoDGD, ApoDGD−Na, and ApoDGD−Ba. For metal-free apoDGD, 0.5 μM apoDGD was incubated with 100 μM PLP in a 950 μL reaction of the following composition: 100 mM TEA−succinate, pH 7.8, 1 unit/mL 2°ADH, and 300 μM NADPH. At time intervals, 95 μL of this binding reaction was transferred to a 100 μL cuvette. The reactions were initiated by addition of 5 μL of AIB and pyruvate to a final concentration of 50 mM AIB and 2 mM pyruvate. The initial rates were recorded and plotted against incubation time. For apoDGD−Na and apoDGD−Ba, the experimental procedures and reaction conditions were similar to those above except 100 mM disodium succinate or 100 mM $BaCl_2$ was used in the reaction solutions.

Rate of PLP Release from Metal-Free DGD, DGD−Na, DGD−K, and DGD−Ba. Metal-free DGD−PLP was made by preincubating apoDGD with 3.5 mM PLP and 100 mM TEA−succinate for 1.5 h, after which 2 μL this DGD−PLP was added to a 950 μL reaction of the following composition: 100 mM TEA−succinate, pH 7.8, 1 unit/mL 2°ADH, and 300 μM NADPH. The reaction for DGD−K was also performed by diluting 1 μL of ~20 mg/mL PLP-loaded enzyme into 10 mL of reaction solution to achieve a higher dilution of PLP. At time intervals, 95 μL of this release reaction was transferred to a 100 μL cuvette and 5 μL of 1M AIB and 40 mM TEA−pyruvate was added to initiate the reactions. The initial rates were recorded and plotted against the incubation time. The experimental procedures were similar to those above for DGD−Na, DGD−K, and DGD−Ba. DGD−Na was made by incubating apoDGD with 100 mM disodium succinate and 200 μM PLP. DGD−K was prepared by incubating apoDGD with 100 mM dipotassium succinate and 20 μM PLP. DGD−Ba was prepared by incubating apoDGD with 100 mM $BaCl_2$ and 500 μM PLP. The reaction solutions had 100 mM disodium succinate for DGD−Na, 100 mM dipotassium succinate for DGD−K, and 100 mM $BaCl_2$ for DGD−Ba.

Rate of K^+, Rb^+, Li^+, Cs^+, and Ba^{2+} Binding to DGD. For K^+, DGD−PLP was made by incubating apoDGD with 500 μM PLP for 2 h. This preincubated DGD was added to solutions containing 100 mM TEA−succinate, varying concentrations of dipotassium succinate, 500 μM PLP, 2 mM TEA−pyruvate, 50 mM AIB, 1 unit/mL 2°ADH, and 200 μM NADPH. Similar experiments were carried out for Rb^+ and Li^+. For Cs^+, the experiment was only carried out with 100 mM dicesium succinate. For Ba^{2+}, the experiment was done with 100 mM $BaCl_2$.

Rate of K^+, Rb^+, Li^+, Cs^+, and Ba^{2+} Release from DGD. For K^+, apoDGD was preincubated with 100 mM TEA−succinate, 500 μM PLP, and 5 mM dipotassium succinate for 2 h, after which 1 μL of this enzyme was added to 1 mL solution of the following composition: 100 mM TEA−succinate, 500 μM PLP, 2 mM TEA−pyruvate, 200 μM NADPH, 1 unit/mL 2°ADH, and 50 mM AIB. The decrease in absorbance at 340 nm was recorded immediately. Similar experiments were carried out for Rb^+, Li^+, Cs^+, and Ba^{2+}. The concentration of metal ion in the incubation with apoDGD was 50 mM for Li^+, 20 mM for Rb^+, 100 mM for Cs^+, and 50 mM for Ba^{2+}.

An alternative method was also employed. For K^+, DGD−K was made by preincubating apoDGD with 2.5 mM dipotassium succinate and 500 μM PLP for 2 h, after which 2 μL of this DGD−K was incubated in a 950 μL reaction of the following composition: 100 mM TEA−succinate, 1 unit/mL 2°ADH, 200 μM NADPH, and 500 μM PLP. In time intervals, 95 μL of this association reaction was transferred to a cuvette, and 5 μL of a TEA−pyruvate and AIB mixture was added to give a final concentration of 2 mM TEA−pyruvate and 50 mM AIB. The reaction rates were recorded and plotted against incubation time. Similar experiments were done with Rb^+, Cs^+, and Ba^{2+}.

RESULTS

DGD has two metal ion binding sites (*7*, *12*). One near the active site (site 1) binds a variety of metal ions (*7*, *13*). The other (site 2) is on the surface of the enzyme, far removed from the active site. Site 2 is occupied by Na^+ in several DGD structures in which Na^+ was not present in the mother liquor (*13*, *15*). Thus, it is highly specific for binding Na^+. In the present studies, it is assumed that site 2 is occupied by Na^+ or that if partial occupancy occurs by other ions at site 2 this does not have an appreciable effect on enzyme activity. This assumption is supported by results presented below showing that cation concentration dependence always accords well to a single-site binding isotherm. Site 2 appears to be structurally very rigid. It is found at the C-terminus of an α-helix that is terminated by the Pro99−Pro100 sequence. These and two other amino acid residues provide carbonyl ligands to the Na^+, while the coordination sphere is completed by a threonine hydroxyl and a water molecule (*7*).

k_{cat}, K_{AIB}, and K_{PLP} of Metal-Free DGD. In the absence of metal ions, it is assumed that DGD follows an ordered bireactant kinetic mechanism (the upper manifold of Scheme 2) for the binding of PLP and AIB. This is a reasonable assumption since X-ray structures with inhibitors show the PLP bound between the protein and inhibitors (*15*). Equation 1 describes the ordered bireactant system with *rapid equilibrium* binding of PLP and AIB (*16*).

$$v_i = V_{max}\frac{[AIB]}{K_{AIB}\left(1+\frac{K_{PLP}}{[PLP]}\right)+[AIB]} \quad (1)$$

Here, v_i is the initial rate, V_{max} is the maximal rate, K_{AIB} is the Michaelis constant, and K_{PLP} is the PLP dissociation constant. In this equation, V_{max} is independent of PLP concentration, while the apparent value of K_{AIB} is dependent

Scheme 2: Mechanism of DGD Catalysis in the Presence of Cation

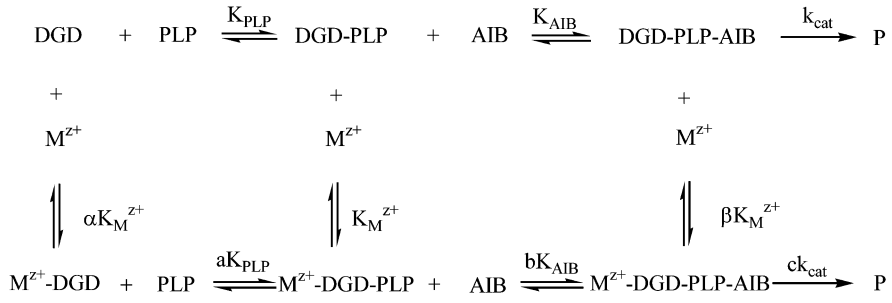

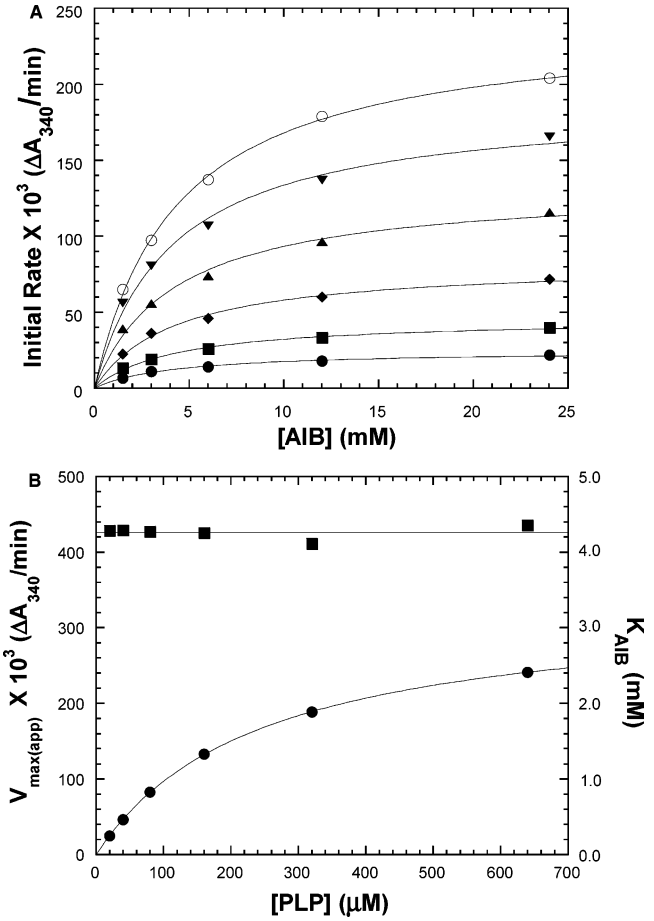

FIGURE 2: Initial velocity saturation curves (A) for the reaction of metal-free DGD with AIB at 20 (●), 40 (■), 80 (◆), 160 (▲), 320 (▼), and 640 μM (○) PLP. The solid curves were the best fit to eq 3. Panel B shows $V_{max(app)}$ (●) and K_{AIB} (■) for metal-free DGD at different concentrations of PLP. $V_{max(app)}$ and K_{AIB} were obtained from curve fitting in panel A. For $V_{max(app)}$, the data (●) were the best fit to eq 4. For K_{AIB}, the data (■) were averaged to be a flat line.

on PLP concentration. The data for six concentrations of PLP were fitted to the Michaelis−Menten equation (Figure 2A). It was found that the apparent values of K_{AIB} were independent of PLP concentration, while V_{max} was dependent on it. This is opposite to the result expected on the basis of eq 1, which describes a rapid equilibrium mechanism.

The initial rates were recorded in the first ~1 min of reaction after addition of AIB, during which the equilibrium between metal-free apoDGD, PLP, and metal-free DGD did not change significantly as deduced from the linear initial rate traces under these conditions. Based on the assumption that the equilibrium between metal-free apoDGD, PLP, and metal-free DGD is not affected by the presence of AIB in the short period of time during which the initial rates were measured (i.e., PLP binding kinetics are slow), eq 2 was derived.

$$v_i = V_{max}\left(\frac{[PLP]}{K_{PLP} + [PLP]}\right)\left(\frac{[AIB]}{K_{AIB} + [AIB]}\right) \qquad (2)$$

Equation 2 describes an ordered bireactant system in which the binding of the first reactant is very slow compared to the binding of the second and to catalysis. Equation 2 can be simplified to eq 3, which has the same form as the Michaelis−Menten equation, and used to fit data in Figure 2A.

$$v_i = V_{max(app)}\frac{[AIB]}{K_{AIB} + [AIB]} \qquad (3)$$

Here, $V_{max(app)}$ is the apparent maximal velocity as given in eq 4.

$$V_{max(app)} = V_{max}\frac{[PLP]}{K_{PLP} + [PLP]} \qquad (4)$$

The apparent maximal velocities obtained from Figure 2A are presented in Figure 2B and least-squares fitted to eq 4, which gives k_{cat}, 3.3 ± 0.1 s^{-1}, and K_{PLP}, 229 ± 37 μM. The AIB dissociation constants obtained from Figure 2A are also presented in Figure 2B and averaged to be 4.1 ± 0.6 mM. The assumption that PLP must bind before AIB and does so slowly is strongly supported by the excellent adherence of the data to eq 2. Scheme 2 also contains cation binding as a component of the kinetic mechanism. As shown, cation binding is proposed to be random with respect to both PLP and AIB. Evidence supporting this proposition is presented below, where it is shown that DGD saturated with PLP and AIB can readily bind various cations. It also appears reasonable on the basis of the lack of overlap between the cation binding site and the active site and the high activity of the metal-free enzyme.

ck_{cat} and bK_{AIB} of Metal-Bound DGD. The initial rates were plotted against AIB concentrations and the curves were least-squares fitted to the Michaelis−Menten equation. The data for four DGD complexes (DGD−Li, DGD−Na, DGD−K, and DGD−Ba) are shown in Figure 3A, and the complete results are presented in Table 1. Compared to metal-free DGD, Li^+, Na^+, Mg^{2+}, Ca^{2+}, and Ba^{2+} all lower the value of k_{cat}, while K^+, Rb^+, NH_4^+, Tl^+, and Cs^+ increase it. The variation of bK_{AIB} with the identity of the cation establishes an energetic coupling between cation and AIB binding.

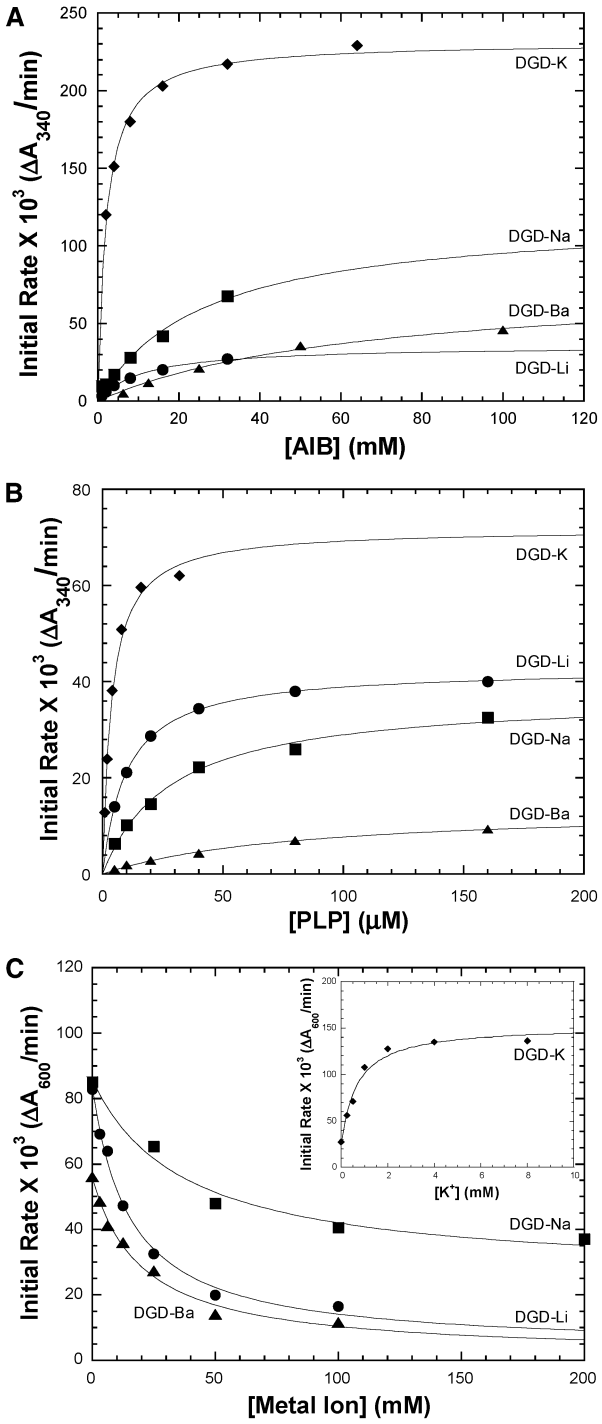

FIGURE 3: Initial velocity saturation curves (A) for the reaction of DGD−Li (●), DGD−Na (■), DGD−K (◆), and DGD−Ba (▲) with AIB. The solid curves through the data are best-fits to the Michaelis−Menten equation. ApoDGD was incubated with 500 μM PLP and 100 mM succinate salt of metal ion (Li^+, Na^+, or K^+) or 100 mM $BaCl_2$ for 1.5 h before addition of substrates. Panel B shows the saturation curves for PLP activation of DGD−Li (●), DGD−Na (■), DGD−K (◆), and DGD−Ba (▲). ApoDGD was incubated with varying concentrations of PLP and 100 mM succinate salt of the metal ion (Li^+, Na^+, or K^+) or 100 mM $BaCl_2$ for 1.5 h before addition of substrates. Panel C shows activation or inhibition saturation curves for metal ion (●, Li^+; ■, Na^+; ◆, K^+ in inset; ▲, Ba^{2+}) binding to DGD. ApoDGD was incubated with 3.5 mM PLP and varying concentrations of the succinate salt of the metal ion (Li^+, Na^+, or K^+) or $BaCl_2$ before the addition of a small amount of AIB to a final concentration of 50 mM.

aK_{PLP}. In the determination of this parameter, only $0.1bK_{AIB}$ was used, and the initial reaction rates were recorded in ~1 min to ensure that the addition of AIB did not change the equilibrium between PLP, apoDGD, and DGD. bK_{AIB} was determined in experiments described above. This small amount of AIB is not expected to change significantly the equilibrium between apoDGD and PLP. Monovalent cations were present at a concentration of 200 mM. Mg^{2+} and Ca^{2+} were present at 100 mM, while Ba^{2+} was present at 50 mM. The initial rates were fitted to eq 5 (Figure 3B).

$$v_i = \frac{V_{max(app)}[PLP]}{aK_{PLP} + [PLP]} \quad (5)$$

Here, v_i is the initial rate, and $V_{max(app)}$ is the apparent maximal velocity. The results are given in Table 1 and show that all monovalent cations facilitate PLP binding to DGD, while divalent cations inhibit binding or facilitate it poorly. The variation of aK_{PLP} with the identity of the cation establishes an energetic coupling between cation and PLP binding.

$\beta K_{M^{z+}}$. The initial rates measured for DGD complexed with Li^+, K^+, Rb^+, NH_4^+, Tl^+, Mg^{2+}, Ca^{2+}, and Ba^{2+} were plotted against cation concentration and fitted to eq 6 (*16*), which describes nonessential activation or inhibition with saturating substrate, to obtain $\beta K_{M^{z+}}$ (the data for Li^+, K^+, and Ba^{2+} are shown in Figure 3C).

$$\frac{V_i}{V_{max}} = \frac{1 + \frac{c[M^{z+}]}{\beta K_{M^{z+}}}}{1 + \frac{[M^{z+}]}{\beta K_{M^{z+}}}} \quad (6)$$

Here, V_i is the initial velocity, V_{max} is the maximal velocity, c is the ratio of the activity of the DGD complex with cation to the activity of metal-free DGD, and $\beta K_{M^{z+}}$ is the concentration of an activator or inhibitor required for half-maximal activation or inhibition.

For Na^+ and Cs^+, 0.5 mM dipotassium succinate was added to the preincubation and reaction solutions to enhance the activity change. The data for these two cations were fitted to eq 7 (*16*) (data for Na^+ is presented in Figure 3C), which describes competitive activation or inhibition in the presence of two ligands that bind to the same site with saturating substrate.

$$\frac{V_i}{V_{max}} = \frac{1 + \frac{c[M^{z+}]}{\beta K_{M^{z+}}} + \frac{c'[M'^{z+}]}{\beta' K'_{M^{z+}}}}{1 + \frac{[M^{z+}]}{\beta K_{M^{z+}}} + \frac{[M'^{z+}]}{\beta' K'_{M^{z+}}}} \quad (7)$$

Here, V_i is the initial velocity, V_{max} is the maximal velocity, c is the ratio of the activity of DGD−PLP complex with Na^+ or Cs^+ to the activity of metal-free DGD, $\beta K_{M^{z+}}$ is the dissociation constant of Na^+ or Cs^+ from DGD−Na or DGD−Cs, c' is the ratio of the activity of DGD−PLP complex with K^+ to the activity of metal-free DGD, and $\beta' K'_{M^{z+}}$ is the dissociation constant of K^+ from DGD−K.

Table 1: Steady-State Kinetic Parameters for DGD Complexes with Various Cations[a]

metal ion	radius (Å)	aK_{PLP} (μM)	bK_{AIB} (mM)	ck_{cat} (s^{-1})	$\alpha K_{M^{z+}}{}^{c}$ (mM)	$K_{M^{z+}}{}^{b}$ (mM)	$\beta K_{M^{z+}}$ (mM)
Li^+	0.60	10.5(0.5)	11(1)	0.86(0.01)	122(39)	5.6(1.5)	15(3)
Na^+	0.95	27(3)	13(1)	1.83(0.03)	40(14)	4.7(1.4)	15(4)
K^+	1.33	3.7(0.3)	2.0(0.2)	10.4(0.2)	86(29)	1.4(0.4)	0.67(0.16)
NH_4^+	1.44	29(7.0)	4.4(0.5)	4.9(0.1)	45(16)	5.7(1.3)	6.1(0.9)
Rb^+	1.48	2.5(0.2)	2.2(0.2)	7.4(0.2)	540(170)	5.9(1.5)	3.2(0.6)
Tl^+	1.49	39(5)	6.6(0.5)	5.22(0.13)	4.4(1.4)	0.75(0.18)	1.2(0.2)
Cs^+	1.69	81(12)	7.3(1.5)	3.8(0.3)	48(18)	17(5)	30(4)
Mg^{2+}	0.65	890(220)	5.8(0.6)	0.076(0.002)	6.0(2.6)	23(7)	32(8)
Ca^{2+}	0.99	240(70)	18(2)	0.05(0.01)	6.5(2.9)	6.8(2.0)	30(7)
Ba^{2+}	1.35	73(18)	66(11)	1.4(0.1)	3.8(1.6)	1.2(0.4)	20(4)

[a] The cation radii were taken from (*31*). The values of K_{PLP}, K_{AIB}, and k_{cat} for metal-free enzyme are as follows: $K_{PLP} = 229 \pm 39$ μM, $K_{AIB} = 4.1 \pm 0.6$ mM, and $k_{cat} = 3.3 \pm 0.1$ s^{-1}. [b] $K_{M^{z+}}$ was calculated from the equation $K_{M^{z+}} = \beta K_{M^{z+}} K_{AIB}/bK_{AIB}$, in which $\beta K_{M^{z+}}$ is the dissociation constant of cation from DGD complex with both cation and AIB, K_{AIB} is AIB dissociation constant of metal-free DGD, and bK_{AIB} is AIB dissociation constant of DGD complex with cation. [c] $\alpha K_{M^{z+}}$ was calculated from the equation $\alpha K_{M^{z+}} = K_{M^{z+}} K_{PLP}/aK_{PLP}$, in which $K_{M^{z+}}$ is cation dissociation constant of DGD complex with cation, K_{PLP} is PLP dissociation constant of metal-free DGD, and aK_{PLP} is PLP dissociation constant of DGD complex with cation.

The results are presented in Table 1. Based on $\beta K_{M^{z+}}$, two additional parameters, $K_{M^{z+}}$ and $\alpha K_{M^{z+}}$, were calculated and are presented in Table 1.

Coenzyme Binding and Release. The activation of metal-free apoDGD by PLP as a function of time is presented in Figure 4A. The curve clearly shows two kinetic processes. This was also seen for apoDGD−K (*14*). The fast phase is essentially complete before the first data point is taken. The second-order rate constants, k_{assoc}, for the slow phase are given in Table 2. The kinetics of PLP binding to apoDGD−Na and apoDGD−Ba are also presented in Figure 4A. They both are monophasic processes, and their second-order binding rate constants are given in Table 2.

Figure 4B presents the activity loss due to release of PLP from metal-free DGD, DGD−Na, DGD−K, and DGD−Ba as a function of time. They are monophasic processes and are fitted to a single-exponential equation. The rate constants (k_{diss}) are given in Table 2.

Metal Ion Binding and Release. Figure 5A presents initial rate traces recorded immediately after addition of varying concentrations of K^+. The curves show large deviations from linearity and clearly indicate that K^+ binding to DGD−PLP is a slow process. The data were fitted to eq 8, where A_{340} is NADPH absorbance at 340 nm, v_i is the initial velocity, v_f is the final velocity, and k_{app} is the apparent rate constant of conversion from metal-free DGD to DGD−K.

$$A_{340} = A_{340}^0 - \left[v_f t + \frac{(v_i - v_f)(1 - e^{(-k_{app}t)})}{k_{app}} \right] \quad (8)$$

The k_{app} values are presented in the inset of Figure 5A. They are not linearly proportional to the K^+ concentration. Saturation of k_{app} with K^+ concentration results from a two-step mechanism, as shown in Scheme 3. A slow step follows rapid equilibrium binding of K^+. The k_{app} values were fitted to eq 9, which is derived from Scheme 3.

$$k_{app} = k_2 \frac{[M^+]}{K_1 + [M^+]} + k_{-2} \quad (9)$$

Here, k_{app} is the apparent rate constant, K_1 is the equilibrium constant in the first rapid equilibrium step, k_2 is the forward reaction rate constant of the second step, and k_{-2} is the reverse rate constant of the second step. The value of $\beta K_{M^{z+}}$ can also be determined using eq 10, in which the values of K_1, k_2, and k_{-2} were determined above.

$$\beta K_{M^{z+}} = K_1 \frac{k_{-2}}{k_2 + k_{-2}} \quad (10)$$

The value of $\beta K_{M^{z+}}$ calculated in this way agrees well with that found in the steady-state assay. Rb^+ gave similar results. For Li^+ (data not shown), only the progress curves at high concentrations can be fitted to eq 8. The value of k_{app} is independent of Li^+ concentration at high concentrations; thus, Li^+ also employs a two-step binding mechanism. Assuming Cs^+ and Ba^{2+} also employ two-step mechanisms, their maximal rate constants (k_{max}) of binding to DGD were determined at high concentrations. The kinetic constants are presented in Table 3.

Figure 5B presents the progress curves of reactions catalyzed by DGD−Li, DGD−K, DGD−Rb, DGD−Cs, and DGD−Ba in the absence of those metal ions in reaction solutions. The curvature indicates the slow release of metal ions from the enzyme. The progress curves were fitted to eq 8. The values of k_{diss} (k_{app} in eq 8) are presented in Table 3. Since the reactions were performed in the presence of 50 mM AIB, k_{diss} is the rate constant for metal ion release from the DGD−PLP−AIB−metal ion complex. An alternative experiment for measuring metal ion release was to incubate DGD−K, DGD−Rb, DGD−Cs, and DGD−Ba in solutions without metal ions or AIB. Plots of enzyme activity vs incubation time were all monophasic and were fitted to a single-exponential equation. The values of k'_{diss} thus obtained (i.e., rate constant for release of metal ion from the DGD−PLP-metal ion complex) are also presented in Table 3.

DISCUSSION

Thermodynamics of Interaction of Cations with DGD. The structure of DGD was solved several years ago. The enzyme exists as a tetramer, which is best described as a dimer of dimers. It provided the first examples of structurally well characterized monovalent cation binding sites (*12*). One cation binding site (site 2) on the surface of the enzyme is specific for Na^+. The other (site 1, Figure 1A) is near the active site and promiscuously binds a variety of cations (*7*, *13*).

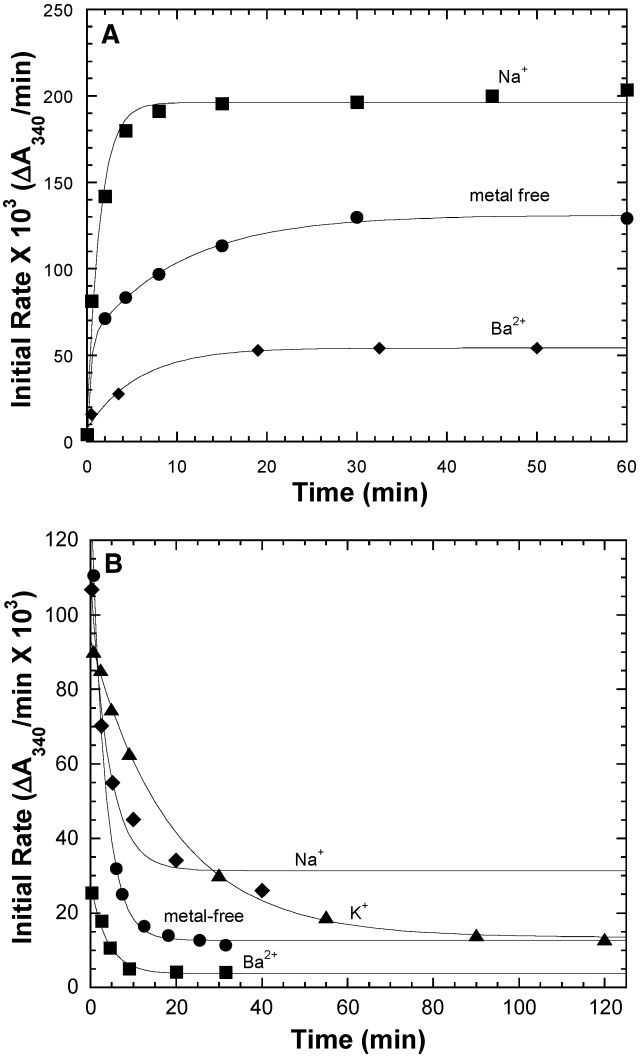

FIGURE 4: Kinetics (A) of the restoration of steady-state activity to metal-free apoDGD (●), apoDGD−Na (■), and apoDGD−Ba (◆) by 100 μM PLP. The reaction of metal-free apoDGD is clearly biphasic, while the reactions of apoDGD−Na and apoDGD−Ba are monophasic. ApoDGD was incubated with 100 mM disodium succinate, 100 mM $BaCl_2$, or without metal for 1.5 h before addition of PLP. Panel B shows kinetics of activity loss for metal-free DGD (●), DGD−Na (◆), DGD−K (▲), and DGD−Ba (■) in the absence of PLP.

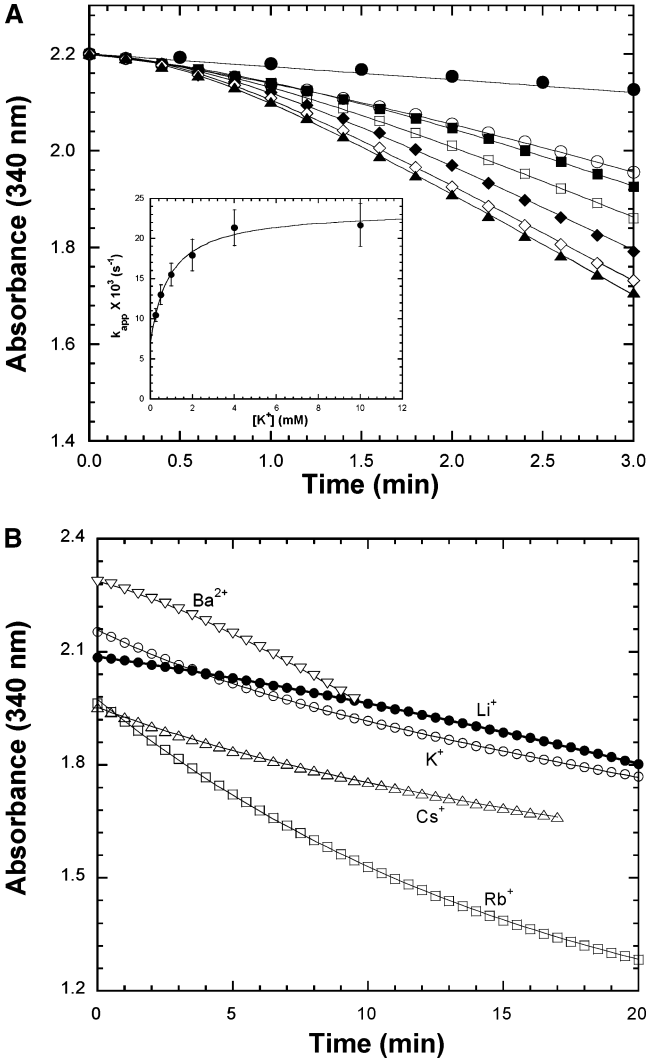

FIGURE 5: Initial velocity curves (A) showing kinetics of DGD activation by 0 (●), 0.25 (○), 0.5 (■), 1 (□), 2 (◆), 4 (◇), and 10 mM (▲) K^+. ApoDGD (0.05 μM) was incubated with 500 μM PLP for 2 h before addition of dipotassium succinate and substrates. The inset shows pseudo-first-order rate constants for K^+ binding obtained from initial velocity curves. The solid curve is the best fit to eq 9. Panel B presents initial velocity curves showing kinetics of Li^+ (●), K^+ (○), Rb^+ (□), Cs^+ (△), and Ba^{2+} (▽) release from DGD. The solid curves are best-fits to eq 8.

Table 2: Kinetic Parameters for PLP Association with and Dissociation from ApoDGD

	k_{assoc}[a] ($M^{-1}\cdot s^{-1}$)	$k_{diss} \times 10^3$ (s^{-1})	calcd K_{PLP} or aK_{PLP}[b] (μM)
metal-free DGD	16(3)	5.0(0.2)	312(60)
DGD−Na	110(20)	3.8(0.6)	34(8)
DGD−K	290(40)[c]	0.92(0.05)	3.2(0.5)
DGD−Ba	29(6)	4.2(0.7)	144(57)

[a] k_{assoc} is the second-order rate constant for PLP association. [b] K_{PLP} or aK_{PLP} calculated from K_{PLP} (or aK_{PLP}) = k_{diss}/k_{assoc}. [c] This number was calculated from data in ref *14*, which were measured under slightly different conditions.

Site 1, near the active site, undergoes a cation-size-dependent switch in structure, which correlates with changes in activity (*7*). The smaller ions, Li^+ and Na^+, both give a similar protein structure, while the larger ions, K^+ and Rb^+, both give a similar structure that is different from that produced by the smaller ions. Thus, there appears to be a two-state, cation-size-dependent switch in protein structure, the switch occurring between Na^+ and K^+.

Scheme 3: Two-Step Binding Mechanism

$$E + M^{z+} \underset{}{\overset{K_1}{\rightleftharpoons}} E\bullet M^{z+} \underset{k_{-2}}{\overset{k_2}{\rightleftharpoons}} E\text{-}M^{z+}$$

The structures of site 1 with K^+ and Na^+ bound are shown in Figure 1 panels A and B, respectively. The K^+ ion is six-coordinate with all ligands being oxygen atoms. Three of these are carbonyl oxygens donated from residues Leu78, Thr303, and Val305. The other three ligands are from the side chain hydroxyl of Ser80, the side chain carboxylate of Asp307, and a water molecule. The most striking structural difference between site 1 and the K^+ channel binding sites is the presence of the negatively charged Asp307 carboxylate as a ligand to the metal ion.

The Na^+ form is five-coordinate with a second water molecule replacing the Thr303 carbonyl and the Ser80

Table 3: Kinetic Parameters for Metal Ion Association with and Dissociation from the DGD−PLP−AIB Complex

metal ion	K_1 (mM)	$k_2 \times 10^3$ (s^{-1})	$k_{-2} \times 10^3$ (s^{-1})	$k_{max} \times 10^3$ [a] (s^{-1})	$k_{diss} \times 10^3$ [b] (s^{-1})	$k'_{diss} \times 10^3$ [c] (s^{-1})	calcd $\beta K_{M^{z+}}$ [d] (mM)
Li^+				4.6(0.5)	0.75(0.17)		
K^+	0.91(0.20)	17(2)	7(2)	24(4)	1.8(0.1)	2.2(0.2)	0.25(0.08)
Rb^+	6.4(2.6)	20(1)	9(1)	29(2)	1.0(0.1)	4.0(0.5)	2.0(0.8)
Cs^+				5.3(0.4)	1.8(0.1)	11(1)	
Ba^{2+}				3.8(0.4)	2.5(0.5)	0.7(0.1)	

[a] k_{max} is the maximal association constant of cation to DGD complex. The values for K^+ and Rb^+ are calculated from the equation $k_{max} = k_2 + k_{-2}$. The values for Li^+, Cs^+, and Ba^{2+} are obtained by fitting the AIB decarboxylation progress curves at 100 mM dilithium succinate, 100 mM dicesium succinate, and 100 mM $BaCl_2$ to eq 8. [b] k_{diss} is the cation dissociation rate constant from the DGD−PLP−AIB complex. [c] k'_{diss} is the cation dissociation rate constant from the DGD-PLP without AIB present. [d] $\beta K_{M^{z+}}$ is calculated from eq 10.

hydroxyl ligands. Thr303 and Ser80 move away from the cation, expanding somewhat the binding site. The expansion and ligand replacement, rather than a simple contraction of the binding site around the smaller cation, is probably required by the steric interactions that would be incurred between the Ser80 side chain and the Thr302 carbonyl were it to contract, as previously proposed (*7*). The Ser80 side chain rotates by ~120° to hydrogen bond to Gln52, thereby displacing Tyr301 from its previous interaction with Gln52.

Thr303 in site 1 directly connects the cation binding site with the phosphate binding site, since the Thr303 side chain hydroxyl donates a hydrogen bond to the PLP phosphate group. The expansion of the binding site around Na^+ changes this hydrogen bonding geometry and is expected to influence PLP binding. One might reasonably expect this Thr303 structural connection between the cation binding site and the PLP phosphate binding site to create an energetic coupling between them. Figure 1C shows the overall cation binding site and active site structural differences caused by the exchange of K^+ for Na^+.

Scheme 2 provides for binding of PLP, cation, and AIB in a generalized kinetic mechanism. AIB binding, which requires the presence of PLP in the active site, is the final binding event in each manifold. This mechanism can account for cooperative interactions between both cation and PLP and cation and AIB binding.

A major goal of this work is to define the constants in Scheme 2 for a variety of cations to understand how variation in cation size, charge, and type influence binding and enzyme reactivity. The upper manifold in Scheme 2 is independent of cation since there is no cation-dependent step. Thus, it is only necessary to determine constants for this manifold once, in the absence of any cation. Figure 2 presents the kinetic data required for determination of K_{PLP}, K_{AIB}, and k_{cat} in the upper manifold. PLP binding was previously documented to be slow (*14*); thus, apoDGD was preincubated for 1.5 h before the addition of AIB to initiate the reaction. On the time scale of the initial velocity measurements, no significant PLP binding occurs even though AIB is expected to promote PLP association due to the ordered nature of their binding. This is demonstrated by the independence of K_{AIB} and the hyperbolic dependence of $V_{max(app)}$ on PLP concentration. Therefore, PLP and AIB binding are *kinetically uncoupled* on the time scale of these measurements.

The values of $K_{PLP} = 229 \pm 39$ μM, $K_{AIB} = 4.1 \pm 0.6$ mM, and $k_{cat} = 3.3 \pm 0.1$ s^{-1} show that the metal-free enzyme is significantly active catalytically compared to the K^+ form (most active) of DGD (Table 1). Thus, the presence of a cation at site 1 is not required for catalytic activity. Sequence alignments with other DGD isozymes, the sequences of which are available in the Genbank database, show that the residues forming site 1 are conserved, while the structures of other homologous enzymes such as ornithine aminotransferase, glutamate semialdehyde aminotransferase, and aminooxononanoate synthase do not indicate a structurally homologous cation binding site (*17*−*19*). The metabolic role, if any, of cation binding site 1 is therefore unclear.

Having determined the constants for the upper manifold in Scheme 2, the remaining constants are specific to each cation being tested. Attempts to measure $\alpha K_{M^{z+}}$ directly by spectroscopic techniques were unsuccessful due to the absence of a measurable signal. $K_{M^{z+}}$ was also problematic to measure since the high concentration of PLP required to saturate apoDGD obscured any spectroscopic signal due to cation binding. On the other hand, $\beta K_{M^{z+}}$ was obtainable from kinetics experiments discussed below. The constants in the lower manifold (aK_{PLP}, bK_{AIB}, and ck_{cat}) are for the metal-saturated enzyme and were measured analogously to those in the upper cation-free manifold except for the presence of saturating cation. aK_{PLP} was measured in experiments in which the concentration of AIB was held at $0.1bK_{AIB}$ (Figure 3B), which was known from previous experiments employing saturating cation and PLP (Figure 3A). The trends in the various kinetic parameters as a function of metal ion radius will be discussed together below.

The values of $\beta K_{M^{z+}}$ were determined in experiments in which cations were mixed with the DGD−PLP−AIB complex and allowed to equilibrate in the initial velocity assay mixture. The known kinetics of metal ion binding (Table 3; discussed below) allowed the choice of the appropriate equilibration time (~15 min after initiation of the reactions) before initial velocities were measured. The results from these experiments are reported in Figure 3C and Table 1. The values of $\alpha K_{M^{z+}}$ and $K_{M^{z+}}$ were obtained from the values of $\beta K_{M^{z+}}$ and the other kinetic parameters given in Table 1. Scheme 2 shows that two thermodynamic boxes including $\beta K_{M^{z+}}$ and one each of $\alpha K_{M^{z+}}$ and $K_{M^{z+}}$ can be constructed. These were used to calculate the values of $\alpha K_{M^{z+}}$ and $K_{M^{z+}}$ reported in Table 1.

A summary of the effects of metal ion radius, type, and charge on the various kinetic parameters is presented in Figure 6A−E, while Figure 6F presents the correlation between the ionic radii of cations and their hydration energies. Excellent linear correlations between ionic radius and hydration energy are observed for both the monovalent and divalent cation series. Thus, the use of ionic radius as

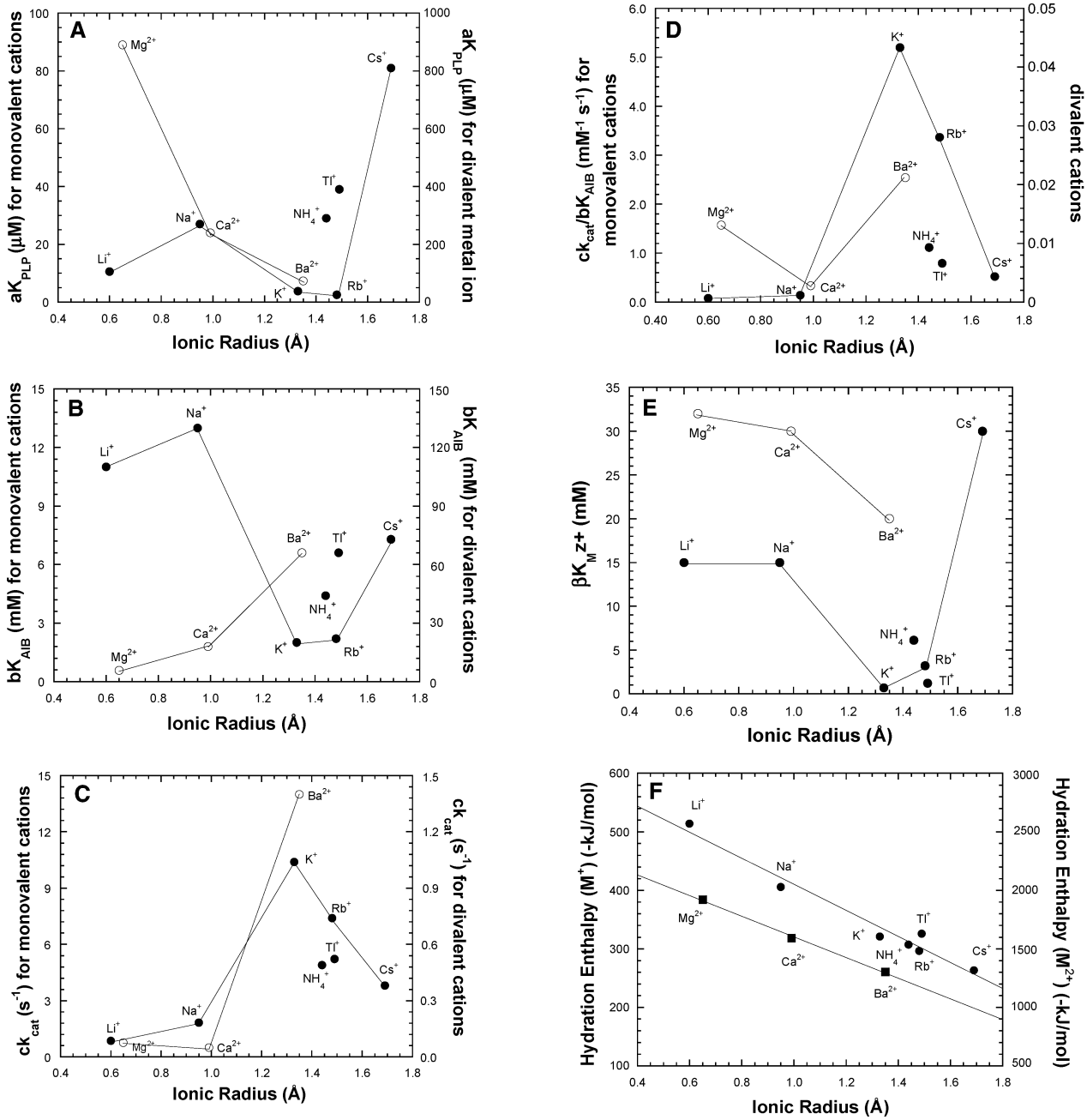

FIGURE 6: aK_{PLP} (A) for the DGD complex with monovalent cations (●) and divalent cations (○) as a function of ionic radius. The scale for the divalent cations is 10-fold that for monovalent cations. Panel B shows bK_{AIB} for the DGD complex with monovalent cations (●) and divalent cations (○) as a function of ionic radius. Panel C shows ck_{cat} for DGD complexes with monovalent cations (●) and divalent cations (○) as a function of ionic radius. Panel D ck_{cat}/bK_{AIB} for DGD complexes with monovalent cations (●) and divalent cations (○) as a function of ionic radius. Panel E shows $\beta K_{M^{z+}}$ for DGD complexes with monovalent cations (●) and divalent cations (○) as a function of ionic radius. Panel F shows cation hydration enthalpy as a function of cation size for monovalent cations (M^+, ●) and divalent cations (M^{2+}, ■). The hydration enthalpy values are from the literature (*32*).

the independent variable in the following analyses implicitly includes hydration effects, where applicable. Of the five kinetic parameters discussed below (aK_{PLP}, bK_{AIB}, ck_{cat}, ck_{cat}/bK_{AIB}, and $\beta K_{M^{z+}}$), the first four are for enzyme that is saturated with cation (Scheme 2) and do not involve its dehydration. The effects observed for these are therefore due to variations in cation size and other properties such as polarizability and geometry (e.g., NH_4^+). The fifth ($\beta K_{M^{z+}}$) does involve dehydration of the cation since it is the dissociation constant for cation binding to the DGD−PLP−AIB complex. For $\beta K_{M^{z+}}$, the linear correlation between ionic radius and hydration energy should be kept in mind.

The effects of metal ion radius, type, and charge on aK_{PLP} are presented in Figure 6A. For the homologous alkali metal ion series, there is a clear optimum in aK_{PLP} when the ionic radius is ~1.4 Å. Thus, K^+ and Rb^+ give the tightest PLP binding with aK_{PLP} values in the low micromolar range. This same trend holds for the other four kinetic parameters shown in Figure 6 and discussed below. The monovalent cations Tl^+ and NH_4^+ give anomalously high aK_{PLP} values when compared to alkali metal ions of similar ionic radius. The divalent alkaline earth metal ions give much poorer binding of PLP when compared to the alkali metal ions of similar ionic radius (note the 10-fold difference in scale of the *Y*-axes

of Figure 6A). From these results, one can conclude that site 1 in DGD is in some way optimized to accommodate alkali metal ions and PLP simultaneously.

The principal mechanism for discrimination between the monovalent alkali metal ions and the divalent alkaline earth metal ions may be the presence of a single carboxylate ion in site 1 for charge compensation. Krasne and Eisenman (*20*) proposed that the discrimination against NH_4^+ in ion channels may be due to the tetrahedral structure of its hydrogens. In DGD, the octahedral geometry of the six oxygen ligands at site 1 would not be expected to interact with NH_4^+ as well as with the spherically symmetric metal ions. The discrimination against Tl^+ binding is more difficult to understand given that the coordination chemistry of K^+ and Tl^+ are quite similar (*21*). Krasne et al. found a similar anomaly with valinomycin, namely, that Tl^+ binds substantially more weakly than predicted from size and K_d's for alkali metal ions, and the opposite with nonactin (*20*, *22*, *23*). They proposed that the greater deformability of the Tl^+ ion vs the alkali metal ions is responsible for its anomalous behavior.

Possibly the most surprising result in Figure 6A is that the value of aK_{PLP} for Li^+ is ~3-fold *lower* than that for Na^+, instead of higher. A close examination of the DGD−Li and DGD−Na structures at site 1 provides a rationale. The switch from the DGD−K to the DGD−Na structures involves replacement of the Thr303 carbonyl ligand to K^+ with a water molecule. In the DGD−Na structure, this water molecule interacts with the Thr303 carbonyl at a distance of 2.7 Å, while in the DGD−Li^+ structure, this distance is lengthened to 3.0 Å because of the shortening of the metal ligand distances around the smaller ion. In the DGD−Li structure, the position of Thr303, of which the side chain hydroxyl hydrogen bonds to the PLP phosphate group, is between those in the DGD−Na and DGD−K structures due to the metal−ligand contractions around Li^+. Thus, some of the strain imposed on the phosphate group by the imperfectly positioned Thr303 side chain in DGD−Na is relieved in DGD−Li. These results support the proposal that the energetic linkage between metal ion and PLP binding is due to the simultaneous Thr303 interaction with the metal through its carbonyl oxygen and PLP phosphate through its side chain hydroxyl.

The dependence of bK_{AIB} on the metal ion radius, type, and charge is shown in Figure 6B. An optimal ionic radius for AIB binding is again found at ~1.4 Å in the alkali metal ion series, and NH_4^+ and Tl^+ show anomalous values. The value of bK_{AIB} for DGD−Li is lower than that for DGD−Na, as for aK_{PLP}. The origin of this effect is likely to be identical to that discussed above, since the orientation of PLP in the active site is expected to affect AIB binding in the Schiff base intermediate, where it is covalently bound to PLP. The most remarkable observation in Figure 6B is that increasing ionic radius for the divalent metal ions gives the opposite trend compared to the monovalent metals ions of similar ionic radius. The origin of this qualitative difference is not clear but may become so once structures for the DGD−divalent metal ion complexes are available.

Figure 6C shows the dependence of ck_{cat}, the rate constant for AIB decarboxylation in the quaternary DGD−metal ion−PLP−AIB complex. A clear optimum is found at K^+, and a similar trend is found for the divalent metal ions, although their rate constants are ~10-fold lower than those for the monovalents of comparable size. The trends in ck_{cat}/bK_{AIB} (Figure 6D), the specificity constant, are very similar for the monovalent cations. Again, an optimum at K^+ is found with Rb^+ a close second at ~60% of the K^+ value. The maximum at K^+ is due to the larger value of ck_{cat} for this ion compared to the others. At present, the detailed structural basis for the optimal DGD catalytic activity with K^+ is not clear.

The binding affinity of cations for the DGD−PLP−AIB complex is represented by $\beta K_{M^{z+}}$. Rapid kinetic studies on DGD show that AIB decarboxylation is the rate-limiting step in the catalytic cycle (*10*); thus, $\beta K_{M^{z+}}$ represents cation binding to the external aldimine intermediate (i.e., AIB−PLP Schiff base). The trends in this parameter with metal ion radius, type, and charge are shown in Figure 6E. K^+ gives the lowest value of $\beta K_{M^{z+}}$. The general trend is very similar to that observed for K^+-specific ion channels (*24*−*29*). The X-ray structure of the K^+ channel shows that six backbone carbonyl groups are used as K^+ ligands, which is quite different than the mixture of carbonyls, carboxylate, hydroxyl, and water ligands found in site 1 of DGD. The commonality between these K^+-specific proteins may simply be that they hold the ligands at the metal−ligand distance most appropriate for K^+ (~2.9 Å). The ion channels must bind and release the metal ions rapidly to be efficient transporters, which may explain the absence of carboxylate ligands. There is a large quantitative difference between K^+ channels and DGD in their discrimination against ions other than K^+. For example, K^+ channels show ~10 000-fold discrimination in favor of K^+ vs Na^+ (*24*−*29*), while there is only ~22-fold discrimination by DGD in $\beta K_{M^{z+}}$. The key to this quantitative difference may be in the higher rigidity of the ligand structure in the K^+ channels vs in DGD.

The trend in $\beta K_{M^{z+}}$ closely follows the trends in the other kinetic parameters discussed above. Therefore, it appears that $\beta K_{M^{z+}}$ values are largely determined by bound state interactions and not dehydration of the cations, which is an integral component of the binding process. This can be understood by consideration of the fact that the same principal factor (i.e., charge density) that causes the smaller ions to interact more strongly with water will also cause them to interact more strongly with the protein ligands, all other factors being equal. The nonlinear discrimination with respect to size observed here is most readily explained by an incomplete flexibility of the protein structure in adapting to the various cation sizes, yielding nonlinear variation in metal−ligand interaction energy.

Kinetics of Interaction of PLP and Cations with DGD. The kinetics of PLP association were measured for metal-free DGD, DGD−Na, DGD−K, and DGD−Ba. The rate constants presented in Table 2 show that all of the metal ions tested increase the rate constant for PLP association with apoDGD. This suggests that the apoDGD active site in the absence of cations has a structure distinct from that with any of the cations bound. There is a surprisingly small difference of 2.6-fold in the effect of Na^+ and K^+ on the association rate constant. A similar result is found with the dissociation rate constant; the k_{diss} for DGD−K is 4-fold lower than that for DGD−Na. This suggests that the transition state for the rate-limiting step for the dissociation of PLP from the DGD−metal ion−PLP complexes is approximately equidistant between reactants and products since the ~10-fold difference in aK_{PLP} for these ions is nearly

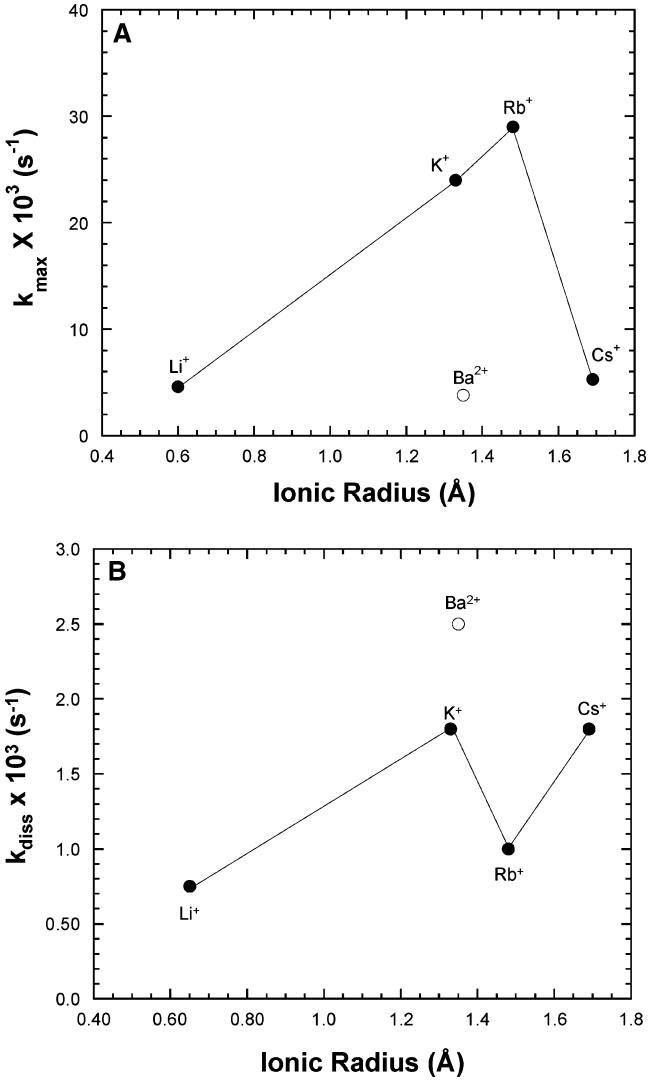

FIGURE 7: Kinetic parameters for the association (A) and dissociation (B) of cations from the DGD−PLP−AIB complexes with monovalent cations (●) and divalent cations (○) as a function of ionic radius.

evenly split between association and dissociation rate constants.

The results of kinetic studies on metal ion binding are given in Table 3 and Figure 7. The primary data analysis presented in Figure 5 shows that K^+ binding follows a two-step preequilibrium mechanism as shown in Scheme 3. Site 1 is not at the immediate surface of the enzyme but is removed from bulk solvent by a layer of amino acid residues. Thus, it is reasonable to expect that cation binding would not follow a simple mechanism. It is not known whether the rapid preequilibrium step is in fact association at the enzyme surface prior to dehydration and penetration into site 1 or binding at site 1 as a prefinal complex. Either appears reasonable given earlier findings with valinomycin and nonactin, which also bind metals in a preequilibrium mechanism although with much faster kinetics (*30*). The data in Table 3 also show that the presence of AIB in the active site slows metal ion dissociation by only 2−6-fold for alkali metal ions. On the other hand, AIB actually increases the dissociation rate constant for Ba^{2+} by 3.6-fold. The association and dissociation rate constants as a function of ionic radius and metal ion type (Figure 7) show that Rb^+ binds most rapidly to the DGD−PLP−AIB complex. The binding of the divalent Ba^{2+} to the complex is substantially slower than expected solely on the basis of ionic radius. The adverse interactions between Ba^{2+} and AIB in the active site are also seen in the 17-fold increase in the equilibrium constant for Ba^{2+} binding ($K_{M^{z+}}$ vs $\beta K_{M^{z+}}$, Table 1) when AIB is present.

In summary, DGD binds a wide variety of cations at site 1 near the active site. The binding of these cations is coupled energetically to the binding of PLP through Thr303. The binding of AIB (bK_{AIB}) displays little discrimination between the presence of K^+ and Rb^+ at site 1. The greatest discrimination between these ions appears in the catalytic constant, k_{cat}, and aK_{PLP}, the PLP binding constant. Yet, for each of these, the discrimination is less than 2-fold. In the homologous series of alkali metal ions, the largest discrimination found is between Cs^+ and Rb^+, where aK_{PLP} is lower for Rb^+ by a factor of 32. This corresponds to a free energy difference of ∼2 kcal/mol, which is much smaller than the ∼6 kcal/mol discrimination between Na^+ and K^+ by K^+-specific ion channels (*24*−*29*). As with nonactin, valinomycin, and the K^+ channels, the binding of both NH_4^+ and Tl^+ show anomalous behavior due to the geometry of the hydrogens in NH_4^+ and the deformability of Tl^+. The divalent alkaline earth cations bind surprisingly well. Discrimination between these and monovalent cations of similar ionic radius is generally only ∼10-fold. The kinetics of PLP binding to DGD are surprisingly slow, and all of the cations tested increase the rate constant for binding. Finally, the association of the cations themselves to the DGD−PLP−AIB complex is slow with $t_{1/2} = 24$ s for the final isomerization step with Rb^+, the fastest binding metal. Dissociation of cations is also relatively slow with $t_{1/2} \approx 12$ min for the DGD−PLP−AIB−Rb^+ complex and $t_{1/2} \approx 3$ min for the DGD−PLP−Rb^+ complex. Thus, metal ion binding is not rapid relative to catalysis ($k_{cat} \approx 10$ s^{-1} with K^+), and control of enzyme activity by intracellular changes in metal ion concentrations would be relatively slow compared to bacterial cell division.

REFERENCES

1. Evan, H. J., and Sorger, G. J. (1966) Role of Mineral Elements with Emphasis on the Univalent Cations, *Annu. Rev. Plant Physiol. 17*, 47−76.
2. Suelter, C. H. (1970) Enzymes Activated by Monovalent Cations, *Science 168*, 789−795.
3. Suelter, C. H. (1974) in *Metal Ions in Biological Systems* (Sigel, H., Ed.) pp 201−251, Marcel Dekker, New York.
4. Woehl, E. U., and Dunn, M. F. (1995) The Roles of Na+ and K+ in Pyridoxal Phosphate Enzyme Catalysis, *Coord. Chem. Rev. 144*, 147−197.
5. Aaslestad, H. G., Bouis, P. J., Jr., Philips, A. T., and Larson, A. D. (1968) in *Pyridoxal Catalysis: Enzymes and Model Systems* (Snell, E. E., Braunstein, A. E., Severin, E. S., and Torchinsky, Y. M., Eds.) pp 470−490, Wiley-Interscience, New York.
6. Adachi, K., Nelson, G. H., Peoples, K. A., DeZwaan, T. M., Skalchunes, A. R., Heiniger, R. W., Shuster, J. R., Hamer, L., and Tanzer, M. M. (2003) Sequence Analysis and Functional Characterization of the Dialkylglycine Decarboxylase Gene Dgd1 from Mycosphaerella Graminicola, *Curr. Genet. 43*, 358−363.
7. Toney, M. D., Hohenester, E., Keller, J. W., and Jansonius, J. N. (1995) Structural and Mechanistic Analysis of Two Refined Crystal Structures of the Pyridoxal Phosphate-Dependent Enzyme Dialkylglycine Decarboxylase, *J. Mol. Biol. 245*, 151−179.
8. Sun, S., Bagdassarian, C. K., and Toney, M. D. (1998) Pre-Steady-State Kinetic Analysis of the Reactions of Alternate Substrates with Dialkylglycine Decarboxylase, *Biochemistry 37*, 3876−3885.

9. Sun, S., Zabinski, R. F., and Toney, M. D. (1998) Reactions of Alternate Substrates Demonstrate Stereoelectronic Control of Reactivity in Dialkylglycine Decarboxylase, *Biochemistry 37*, 3865−3875.
10. Zhou, X., Jin, X., Medhekar, R., Chen, X., Dieckmann, T., and Toney, M. D. (2001) Rapid Kinetic and Isotopic Studies on Dialkylglycine Decarboxylase, *Biochemistry 40*, 1367−1377.
11. Liu, W., Rogers, C. J., Fisher, A. J., and Toney, M. D. (2002) Aminophosphonate Inhibitors of Dialkylglycine Decarboxylase: Structural Basis for Slow Binding Inhibition, *Biochemistry 41*, 12320−12328.
12. Toney, M. D., Hohenester, E., Cowan, S. W., and Jansonius, J. N. (1993) Dialkylglycine Decarboxylase Structure: Bifunctional Active Site and Alkali Metal Sites, *Science 261*, 756−759.
13. Hohenester, E., Keller, J. W., and Jansonius, J. N. (1994) An Alkali Metal Ion Size-Dependent Switch in the Active Site Structure of Dialkylglycine Decarboxylase, *Biochemistry 33*, 13561−13570.
14. Zhou, X., Kay, S., and Toney, M. D. (1998) Coexisting Kinetically Distinguishable Forms of Dialkylglycine Decarboxylase Engendered by Alkali Metal Ions, *Biochemistry 37*, 5761−5769.
15. Malashkevich, V. N., Strop, P., Keller, J. W., Jansonius, J. N., and Toney, M. D. (1999) Crystal Structures of Dialkylglycine Decarboxylase Inhibitor Complexes, *J. Mol. Biol. 294*, 193−200.
16. Segel, I. H. (1993) *Enzyme Kinetics: Behavior and Analysis of Rapid Equilibrium and Steady-State Enzyme Systems*, John Wiley & Sons, New York.
17. Shen, B. W., Hennig, M., Hohenester, E., Jansonius, J. N., and Schirmer, T. (1998) Crystal Structure of Human Recombinant Ornithine Aminotransferase, *J. Mol. Biol. 277*, 81−102.
18. Hoober, J. K., Kahn, A., Ash, D. E., Gough, S., and Kannangara, C. G. (1988) Biosynthesis of Delta-Aminolevulinate in Greening Barley Leaves. Ix. Structure of the Substrate, Mode of Gabaculine Inhibition, and the Catalytic Mechanism of Glutamate 1-Semialdehyde Aminotransferase, *Carlsberg Res. Commun. 53*, 11−25.
19. Alexeev, D., Alexeeva, M., Baxter, R. L., Campopiano, D. J., Webster, S. P., and Sawyer, L. (1998) The Crystal Structure of 8-Amino-7-Oxononanoate Synthase: A Bacterial Plp-Dependent, Acyl-Coa-Condensing Enzyme, *J. Mol. Biol. 284*, 401−419.
20. Szabo, G., Eisenman, G., Laprade, R., Ciani, S. M., and Krasne, S. (1973) Experimentally Observed Effects of Carriers on the Electrical Properties of Bilayer Membranes--Equilibrium Domain. With a Contribution on the Molecular Basis of Ion Selectivity, *Membranes 2*, 179−328.
21. Cotton, F. A., and Wilkinson, G. (1988) *Advanced Inorganic Chemistry*, 5th ed., Wiley, New York.
22. Krasne, S., and Eisenman, G. (1976) Influence of Molecular Variations of Ionophore and Lipid on the Selective Ion Permeability of Membranes: I. Tetranactin and the Methylation of Nonactin-Type Carriers, *J. Membr. Biol. 30*, 1−44.
23. Eisenman, G., Krasne, S., and Ciani, S. (1975) The Kinetic and Equilibrium Components of Selective Ionic Permeability Mediated by Nactin- and Valinomycin-Type Carriers Having Systematically Varied Degrees of Methylation, *Ann. N. Y. Acad. Sci. 264*, 34−60.
24. Hille, B. (1973) Potassium Channels in Myelinated Nerve. Selective Permeability to Small Cations, *J. Gen. Physiol. 61*, 669−686.
25. Gay, L. A., and Stanfield, P. R. (1978) The Selectivity of the Delayed Potassium Conductance of Frog Skeletal Muscle Fibers, *Pflugers Arch. 378*, 177−179.
26. Reuter, H., and Stevens, C. F. (1980) Ion Conductance and Ion Selectivity of Potassium Channels in Snail Neurones, *J. Membr. Biol. 57*, 103−118.
27. Hagiwara, S., and Takahashi, K. (1974) The Anomalous Rectification and Cation Selectivity of the Membrane of a Starfish Egg Cell, *J. Membr. Biol. 18*, 61−80.
28. Gorman, A. L., Woolum, J. C., and Cornwall, M. C. (1982) Selectivity of the Ca2+-Activated and Light-Dependent K+ Channels for Monovalent Cations, *Biophys. J. 38*, 319−322.
29. Neyton, J., and Miller, C. (1988) Potassium Blocks Barium Permeation through a Calcium-Activated Potassium Channel, *J. Gen. Physiol. 92*, 549−567.
30. Grell, E., Funck, T., and Eggers, F. (1975) Structure and Dynamic Properties of Ion-Specific Antibiotics, *Membranes 3*, 1−126.
31. Glusker, J. P. (1991) Structural Aspects of Metal Liganding to Functional Groups in Proteins, *Adv. Protein Chem. 42*, 1−76.
32. Richens, D. T. (1997) *The Chemistry of Aqua Ions*, John Wiley & Sons, New York.

BI035854L